INTERNATIONAL JOURNAL OF NUMERICAL MODELLING : ELECTRONIC NETWORKS, DEVICES AND FIELDS,
Vol. 4, 63–73 (1991)

COMPARISON BETWEEN DIFFERENT FORMULATIONS OF THE TRANSVERSE RESONANCE FIELD-MATCHING TECHNIQUE FOR THE THREE-DIMENSIONAL ANALYSIS OF METAL-FINNED WAVEGUIDE RESONATORS*

JENS BORNEMANN

Department of Electrical and Computer Engineering, University of Victoria, Victoria, BC, Canada, V8W 3P6

SUMMARY

Two different formulations of the transverse resonance field-matching technique are applied to evaluate the modal spectrum of metal-finned waveguide structures. In the theoretical treatment, Method 1 uses boundary conditions prior to interface relations and allows the number of expansion terms to be selected according to the dimensions of the cross-section subregions. Method 2 imposes boundary and interface conditions in reversed order but requires the same number of expansion terms to be used in various subregions. The two procedures are then compared with respect to their influence on the modal scattering matrix computation of metal-finned waveguide resonators. Method 2 shows excellent agreement with measurements, but it is restricted to configurations with relatively thin fins and moderate slot widths. Although Method 1 may be applied to more general structures, this procedure requires a higher computational effort and leads to slightly different results. However, it constitutes a powerful PC-operational alternative whenever an extended precision compiler, as required for Method 2, is not available.

1. INTRODUCTION

Metal-finned and ridged waveguide structures are well known to combine the advantages of broadband fundamental-mode operation, low characteristic impedance, and the possibility of low-cost *E*-plane circuit integration utilizing metal-etching techniques and split-block housing fabrication. While some of the papers published in the area of numerical modelling of ridged waveguides reported cross-sectional solutions to determine the mode spectrum including the fundamental-mode characteristic impedance,[1–5] others focused on the design of components,[6–8] and the combination of the two-dimensional data with equivalent circuit theory.[9,13]

The amount of cutoff frequency reduction compared with a rectangular waveguide of the same housing dimensions makes the ridged waveguide suitable for evanescent-mode filter applications. The ridged resonator sections in these components may be realized by *E*-plane screws,[10–12] thin non-touching *E*-plane fins supported by a dielectric substrate,[17] or by pure metal fins as will be presented in this contribution. Compared with the non-touching fin configuration, the all-metal fin design has the advantages of a simpler field theory treatment and lower losses because of the absence of hybrid modes and dielectric material, respectively. The tuning screw structure[10–12] is limited to the microwave region and cannot be applied at millimetre waves where the diameter of the tuning device approaches the cross-section dimension of the evanescent-mode waveguide.

Various field theoretical procedures have been reported for the characterization of three-dimensional finned waveguide discontinuities.[14–19] Different two-dimensional treatments for the evaluation of the modal spectrum of the finned waveguide have been investigated with respect to their influence on the three-dimensional response.[20] It has been shown that the method used to incorporate boundary conditions and interface relations in the algorithm can affect the computation of the overall response of circuits. Owing to lack of space in Reference 20, however, details about the numerical modelling process itself could not be revealed.

Therefore, this paper focuses on a detailed presentation of different formulations of the transverse resonance field-matching technique for the three-dimensional analysis of metal-finned waveguide resonators (see Figure 1). It is intended to not only introduce the reader to the basic steps

*Invited Paper.

0894–3370/91/010063–11$05.50

Received 11 June 1990
Revised 18 February 1991

of the different approaches, but also to provide the design engineer with guidelines regarding the applicability and accuracy of the techniques. In detail, the two numerical approaches for the evaluation of the finned waveguide mode spectrum are:

—*Method 1:* The classic modal analysis[3,21] where the boundary conditions are introduced at the beginning of the formulation, and the interface relations are applied later to yield the characteristic matrix equation for the condition of transverse resonance.

—*Method 2:* The approach which assumes a wave propagation perpendicular to the axial direction.[22–24] Here the interface relations are imposed first while the boundary conditions are incorporated at the end, after certain manipulations and substitutions have been made. Finally, a resonance condition similar to the more general procedure presented in Reference 25 is obtained.

Although the resulting eigenfunctions of the finned waveguide cross-section derived from both methods have the same form and, theoretically, should lead to identical values, the numerical procedures produce slightly different results because of the different manipulations of the basic equations and their individual implementation in a software package. Instead of comparing columns of cutoff frequencies, separation constants and eigenvectors for the two-dimensional cases, the different transverse resonance formulations are investigated with respect to their influence on the three-dimensional response. The advantages and disadvantages are discussed in order to help a potential user to choose the adequate numerical modelling technique for his metal-finned waveguide application. The computed results are compared with measurements of a three-resonator evanescent-mode filter structure.

2. THEORY

This chapter first presents the basic steps of the mode-matching technique in propagation direction. It leads to the generalized (modal) scattering matrix formulation of a discontinuity and is common to both tranverse resonance field-matching techniques which will be described in Sections 2.2 and 2.3.

2.1. *Mode-matching technique in propagation direction*

The rigorous field theory treatment of the discontinuity problem shown in Figure 2 requires all field components and mode coupling effects to be considered. Hence, the electromagnetic field in subregions $i = 0$, I, II (see Figure 2(a))

$$\mathbf{E}^i = \nabla \times (A^i_{hz}\mathbf{e}_z) + \frac{1}{\mathrm{j}\omega\epsilon_0}\nabla \times \nabla \times (A^i_{ez}\mathbf{e}_z) \tag{1}$$

$$\mathbf{H}^i = \nabla \times (A^i_{ez}\mathbf{e}_z) - \frac{1}{\mathrm{j}\omega\mu_0}\nabla \times \nabla \times (A^i_{hz}\mathbf{e}_z) \tag{2}$$

can be derived from vector potential components

$$A^i_{hz} = \sum_{q=1}^{N_h} \sqrt{Z^i_{hq}}\, T^i_{hq}(x,y)\{F^i_{hq}\exp(-\mathrm{j}k^i_{zhq}z) + B^i_{hq}\exp(+\mathrm{j}k^i_{zhq}z)\} \tag{3}$$

$$A^i_{ez} = \sum_{p=1}^{N_e} \sqrt{Y^i_{ep}}\, T^i_{ep}(x,y)\{F^i_{ep}\exp(-\mathrm{j}k^i_{zep}z) - B^i_{ep}\exp(+\mathrm{j}k^i_{zep}z)\} \tag{4}$$

where $F^i_{h,e}$, $B^i_{h,e}$ are the wave amplitudes of the forward and backward travelling waves, respectively, $k^i_{zh,e}$ are the propagation constants related to the cutoff frequencies $f^i_{ch,e}$ by

$$k^i_{zh,e} = \omega^2\mu_0\epsilon_0\sqrt{1 - (f^i_{ch,e}/f)^2} \tag{5}$$

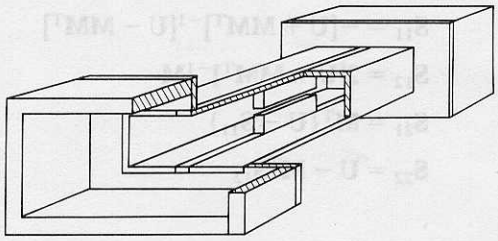

Figure 1. Finned waveguide resonator within an evanescent-mode waveguide section

and Z_h^i and Y_e^i are the wave impedances and admittances of TE and TM modes, respectively.[16] $T_{h,e}^i$ are the cross-section eigenfunctions according to the boundary conditions. For the rectangular waveguide regions $i = 0$, I, they read (see Figure 2(b))

$$T_{hq}^i(x, y) = A_q^i \cos\left\{(2m-1)\pi \begin{bmatrix}(x+\Delta a)/a_1\\ x/a\end{bmatrix}\right\} \cos\left\{2n\pi \begin{bmatrix}(y+\Delta b)/b_1\\ y/b\end{bmatrix}\right\} \Big/ \sqrt{1+\delta on} \tag{6}$$

$$T_{ep}^i(x, y) = D_p^i \sin\left\{(2m-1)\pi \begin{bmatrix}(x+\Delta a)/a_1\\ x/a\end{bmatrix}\right\} \sin\left\{2n\pi \begin{bmatrix}(y+\Delta b)/b_1\\ y/b\end{bmatrix}\right\} \tag{7}$$

The coefficients in the cross-section functions, e.g. A_q^i, D_p^i in (6), (7), are normalized by

$$\int_{F^i} [\nabla T_{hq,\,ep}^i]^2 \, \mathrm{d}F = 1 \tag{8}$$

so that the power carried by a mode through the cross-section F^i is

$$P_{hq,\,ep}^i = \begin{cases} 1W & \text{for propagating modes} \\ \mathrm{j}W & \text{for evanescent TE modes} \\ -\mathrm{j}W & \text{for evanescent TM modes} \end{cases} \tag{9}$$

if the corresponding wave amplitude equals $1\sqrt{W}$.

Matching the tangential field components of regions i and $i + 1$ at their common interface yields the modal scattering matrix of the discontinuity

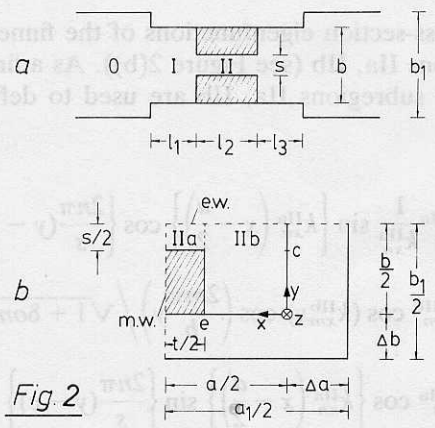

Figure 2. Dimensions of finned waveguide resonator. (a) Sideview; (b) cross-sections and subregions for the field theory treatment (e.w. = electric wall, m.w. = magnetic wall)

$$\mathbf{S}_{11} = -[\mathbf{U} + \mathbf{M}\mathbf{M}^{\mathrm{T}}]^{-1}[\mathbf{U} - \mathbf{M}\mathbf{M}^{\mathrm{T}}] \tag{10}$$

$$\mathbf{S}_{12} = 2[\mathbf{U} + \mathbf{M}\mathbf{M}^{\mathrm{T}}]^{-1}\mathbf{M} \tag{11}$$

$$\mathbf{S}_{21} = \mathbf{M}^{\mathrm{T}}\{\mathbf{U} - \mathbf{S}_{11}\} \tag{12}$$

$$\mathbf{S}_{22} = \mathbf{U} - \mathbf{M}^{\mathrm{T}}\mathbf{S}_{12} \tag{13}$$

where

$$\mathbf{M} = \begin{bmatrix} \operatorname{diag}\{\sqrt{Y_{hq}^{i}}\}\mathbf{J}_{\mathrm{HH}} \operatorname{diag}\{\sqrt{Z_{hu}^{i+1}}\} & \mathbf{0} \\ \operatorname{diag}\{\sqrt{Y_{ep}^{i}}\}\mathbf{J}_{\mathrm{EH}} \operatorname{diag}\{\sqrt{Z_{hu}^{i+1}}\} & \operatorname{diag}\{\sqrt{Y_{ep}^{i}}\}\mathbf{J}_{\mathrm{EE}} \operatorname{diag}\{\sqrt{Z_{ev}^{i+1}}\} \end{bmatrix} \tag{14}$$

In (10)–(14), T means transposed, **U** is the unit matrix, and diag {} denotes a diagonal matrix. The coupling matrices are given by

$$(\mathbf{J}_{\mathrm{HH}})_{qu} = \int_{F^{i+1}} (\nabla T_{hq}^{i} \times \mathbf{e}_z)(\nabla T_{hu}^{i+1} \times \mathbf{e}_z)\, \mathrm{d}F \tag{15}$$

$$(\mathbf{J}_{\mathrm{EH}})_{pu} = \int_{F^{i+1}} (-\nabla T_{ep}^{i})(\nabla T_{hu}^{i+1} \times \mathbf{e}_z)\, \mathrm{d}F \tag{16}$$

$$(\mathbf{J}_{\mathrm{EE}})_{pv} = \int_{F^{i+1}} (\nabla T_{ep}^{i})(\nabla T_{ev}^{i+1})\, \mathrm{d}F \tag{17}$$

It should be noted that the fourth possibility of coupling the cross-section functions results in $(\mathbf{J}_{\mathrm{HE}})_{qv} = 0$ since it involves integration over the vanishing tangential electric field along the boundary of region $i + 1$.[16] As a result, submatrix $\mathbf{M}_{12}$ in (14) vanishes. For further algorithms leading to the modal scattering matrix of discontinuities of finite lengths and cascaded structures, the reader is referred to Reference 16.

As can be seen from (10)–(13) together with (14)–(17), the wave impedances, which are related to the eigenmode cutoff frequencies, as well as the cross-section eigenfunctions $T_{h,e}^{i}$ directly influence the modal scattering matrix calculation of the discontinuity rectangular to finned waveguide.

2.2. *Method* 1

In order to determine the cross-section eigenfunctions of the finned or ridged waveguide, region II is divided into two subregions IIa, IIb (see Figure 2(b)). As a first step of this formulation, the given boundary conditions of subregions IIa, IIb are used to define the x,y-dependence of the cross-section functions.

$$T_{hu}^{\mathrm{IIa}} = \sum_{n=0}^{N} A_n^{\mathrm{IIa}} \frac{1}{k_{xn}^{\mathrm{IIa}}} \sin\left\{k_{xn}^{\mathrm{IIa}}\left(x - \frac{a}{2}\right)\right\} \cos\left\{\frac{2n\pi}{s}(y - c)\right\} \Big/ \sqrt{1 + \delta o n} \tag{18}$$

$$T_{hu}^{\mathrm{IIb}} = \sum_{m=0}^{M} A_m^{\mathrm{IIb}} \cos(k_{xm}^{\mathrm{IIb}} x) \cos\left(\frac{2m\pi}{b} y\right) \Big/ \sqrt{1 + \delta o m} \tag{19}$$

$$T_{ev}^{\mathrm{IIa}} = \sum_{n=1}^{N} D_n^{\mathrm{IIa}} \cos\left\{k_{xn}^{\mathrm{IIa}}\left(x - \frac{a}{2}\right)\right\} \sin\left\{\frac{2n\pi}{s}(y - c)\right\} \tag{20}$$

$$T_{ev}^{\mathrm{IIb}} = \sum_{m=1}^{M} D_m^{\mathrm{IIb}} \frac{1}{k_{xm}^{\mathrm{IIb}}} \sin(k_{xm}^{\mathrm{IIb}} x) \sin\left(\frac{2m\pi}{b} y\right) \tag{21}$$

with

$$\begin{bmatrix}(k_{xn}^{\mathrm{IIa}})^2\\(k_{xn}^{\mathrm{IIb}})^2\end{bmatrix} = \omega^2\mu_0\epsilon_0 - \begin{bmatrix}\left(\dfrac{2n\pi}{s}\right)^2\\\left(\dfrac{2n\pi}{b}\right)^2\end{bmatrix} \tag{22}$$

Since from (22) it follows that k_x is either real or purely imaginary, a division by k_x is introduced in (18) and (21) to obtain real cross-section functions. It should also be noted that (22) is valid only at the cutoff frequencies of the finned waveguide where the propagation constant k_z vanishes. Once a cutoff frequency is determined, the frequency dependence of the related k_z is given by (5).

In the second step, the subregion functions (18)–(21) as well as their derivatives with respect to x are matched at the common interface at $x = e$ (Figure 2(b)). This leads to the interface relations which consists of two sets of two matrix equations each. In order to keep the characteristic matrix to be derived small, e.g. $N \times N$ instead of $(M + N) \times (M + N)$, each set can be rearranged in the following way:

$$\mathbf{A}^{\mathrm{IIb}} = -\frac{4}{b}\,\mathrm{diag}\left\{\frac{1}{k_{xm}^{\mathrm{IIb}}\sin(k_{xm}^{\mathrm{IIb}}e)}\right\}\mathbf{J}_c\,\mathrm{diag}\left\{\cos\left(k_{xn}^{\mathrm{IIa}}\frac{t}{2}\right)\right\}\mathbf{A}^{\mathrm{IIa}} \tag{23}$$

$$\left[\frac{s}{4}\,\mathrm{diag}\left\{\frac{\sin\left(k_{xn}^{\mathrm{IIa}}\dfrac{t}{2}\right)}{k_{xn}^{\mathrm{IIa}}}\right\} - \frac{4}{b}\mathbf{J}_c^{\mathrm{T}}\,\mathrm{diag}\left\{\frac{\cot(k_{xm}^{\mathrm{IIb}}e)}{k_{xm}^{\mathrm{IIb}}}\right\}\mathbf{J}_c\,\mathrm{diag}\left\{\cos\left(k_{xn}^{\mathrm{IIa}}\frac{t}{2}\right)\right\}\right]\mathbf{A}^{\mathrm{IIa}} = 0 \tag{24}$$

$$\mathbf{D}^{\mathrm{IIb}} = \frac{4}{b}\,\mathrm{diag}\left\{\frac{k_{xm}^{\mathrm{IIb}}}{\sin(k_{xm}^{\mathrm{IIb}}e)}\right\}\mathbf{J}_s\,\mathrm{diag}\left\{\cos\left(k_{xn}^{\mathrm{IIa}}\frac{t}{2}\right)\right\}\mathbf{D}^{\mathrm{IIa}} \tag{25}$$

$$\left[\frac{s}{4}\,\mathrm{diag}\left\{k_{xn}^{\mathrm{IIa}}\sin\left(k_{xn}^{\mathrm{IIa}}\frac{t}{2}\right)\right\} - \frac{4}{b}\mathbf{J}_s^{\mathrm{T}}\,\mathrm{diag}\left\{\frac{k_{xm}^{\mathrm{IIb}}}{\tan(k_{xm}^{\mathrm{IIb}}e)}\right\}\mathbf{J}_s\,\mathrm{diag}\left\{\cos\left(k_{xn}^{\mathrm{IIa}}\frac{t}{2}\right)\right\}\right]\mathbf{D}^{\mathrm{IIa}} = 0 \tag{26}$$

where

$$(\mathbf{J}_c)_{mn} = \int_c^{b/2} \frac{\cos\left(\dfrac{2m\pi}{b}y\right)}{\sqrt{1+\delta om}}\,\frac{\cos\left\{\dfrac{2n\pi}{s}(y-c)\right\}}{\sqrt{1+\delta on}}\,\mathrm{d}y \tag{27}$$

$$(\mathbf{J}_s)_{mn} = \int_c^{b/2} \sin\left(\frac{2m\pi}{b}y\right)\sin\left\{\frac{2n\pi}{s}(y-c)\right\}\mathrm{d}y \tag{28}$$

The terms in brackets in (24) and (26) represent the characteristic matrices for TE and TM modes, respectively, which have to be solved for the zeros of the determinants by varying the frequency f. Every zero corresponds to a cutoff frequency of the finned waveguide eigenmode spectrum and a set of separation constants k_x. Solving for the coefficients vectors **A**, **D** and applying the condition (8) finally leads to the cross-section eigenfunction formulations of TE modes [(18) + (19)] and TM modes [(20) + (21)] of the finned waveguide. One advantage of this method is that the size of the characteristic matrix equals the number N of expansion terms in the smaller subregion IIa. For a given maximum number of M the ratio N/M is usually very close to the dimension ratio s/b. In this case, 'the field behaves reasonably well across the junction'.[26]

2.3. *Method* 2

Contrary to the formulation with standing waves in Section 2.2, Method 2 defines propagating partial waves for the x-dependence of the subregion functions in cross-sections i = IIa, IIb (see Figure 2(b)):

$$Q_{hn}^{i} = A_n^i \exp(+\mathrm{j}k_{xn}^i x) + B_n^i \exp(-\mathrm{j}k_{xn}^i x) \tag{29}$$

in (18), (19) and

$$P_{en}^{i} = \frac{1}{\mathrm{j}k_{xn}^i}[C_n^i \exp(+\mathrm{j}k_{xn}^i x) - D_n^i \exp(-\mathrm{j}k_{xn}^i x)] \tag{30}$$

in (20), (21). The y-dependence as well as the separation constants (22) remain the same.

By matching these partial waves and their derivatives with respect to x (P_{hn}^i, Q_{en}^i; see Reference 22) at the interface at $x = e$, transforming them to the left (region IIa) and right (region IIb) boundaries and, as the last step in this formulation, inserting the boundary conditions at $x = 0$, $a/2$ as the transverse resonance condition[22] two sets of matrix equations are obtained.

$$\mathbf{P}_{h(x=a/2)}^{\mathrm{IIa}} = \left[\frac{b}{4}\,\mathrm{diag}\left\{\cos\left(k_{xn}^{\mathrm{IIa}}\frac{t}{2}\right)\right\}\mathbf{J}_c^{-1}\,\mathrm{diag}\{-k_{xn}^{\mathrm{IIb}}\sin(k_{xn}^{\mathrm{IIb}}e)\} + \frac{4}{s}\,\mathrm{diag}\left\{-k_{xn}^{\mathrm{IIa}}\sin\left(k_{xn}^{\mathrm{IIa}}\frac{t}{2}\right)\right\}\mathbf{J}_c\,\mathrm{diag}\{\cos(k_{xn}^{\mathrm{IIb}}e)\}\right]\mathbf{Q}_{h(x=0)}^{\mathrm{IIb}} \tag{31}$$

$$\left[\frac{b}{4}\,\mathrm{diag}\left\{\frac{1}{k_{xn}^{\mathrm{IIa}}}\sin\left(k_{xn}^{\mathrm{IIa}}\frac{t}{2}\right)\right\}\mathbf{J}_c^{-1}\,\mathrm{diag}\{-k_{xn}^{\mathrm{IIb}}\sin(k_{xn}^{\mathrm{IIb}}e)\} + \frac{4}{s}\,\mathrm{diag}\left\{\cos\left(k_{xn}^{\mathrm{IIa}}\frac{t}{2}\right)\right\}\mathbf{J}_c\,\mathrm{diag}\{\cos(k_{xn}^{\mathrm{IIb}}e)\}\right]\mathbf{Q}_{h(x=0)}^{\mathrm{IIb}} = 0 \tag{32}$$

$$\mathbf{P}_{e(x=a/2)}^{\mathrm{IIa}} = \left[\frac{b}{4}\,\mathrm{diag}\left\{\cos\left(k_{xn}^{\mathrm{IIa}}\frac{t}{2}\right)\right\}\mathbf{J}_s^{-1}\,\mathrm{diag}\left\{\frac{1}{k_{xn}^{\mathrm{IIb}}}\sin\left(k_{xn}^{\mathrm{IIb}}e\right)\right\} + \frac{4}{s}\,\mathrm{diag}\left\{\frac{1}{k_{xn}^{\mathrm{IIa}}}\sin\left(k_{xn}^{\mathrm{IIa}}\frac{t}{2}\right)\right\}\mathbf{J}_s\,\mathrm{diag}\{\cos(k_{xn}^{\mathrm{IIb}}e)\}\right]\mathbf{Q}_{e(x=0)}^{\mathrm{IIb}} \tag{33}$$

$$\left[\frac{b}{4}\,\mathrm{diag}\left\{-k_{xn}^{\mathrm{IIa}}\sin\left(k_{xn}^{\mathrm{IIa}}\frac{t}{2}\right)\right\}\mathbf{J}_s^{-1}\,\mathrm{diag}\left\{\frac{1}{k_{xn}^{\mathrm{IIb}}}\sin(k_{xn}^{\mathrm{IIb}}e)\right\} + \frac{4}{s}\,\mathrm{diag}\left\{\cos\left(k_{xn}^{\mathrm{IIa}}\frac{t}{2}\right)\right\}\mathbf{J}_s\,\mathrm{diag}\{\cos(k_{xn}^{\mathrm{IIb}}e)\}\right]\mathbf{Q}_{e(x=0)}^{\mathrm{IIb}} = 0 \tag{34}$$

with matrices $\mathbf{J}_c$, $\mathbf{J}_s$ according to (27), (28).

After solving for the zeros of the determinants of the characteristic matrices in (32), (34), applying (8) and expressing A_n^i, B_n^i, C_n^i, D_n^i in (29), (30) as a function of $\mathbf{P}_{h(x=a/2)}^{\mathrm{IIa}}$, $\mathbf{Q}_{h(x=0)}^{\mathrm{IIb}}$, $\mathbf{P}_{e(x=a/2)}^{\mathrm{IIa}}$, $\mathbf{Q}_{e(x=0)}^{\mathrm{IIb}}$, the cross-section eigenfunctions of the finned waveguide turn out to have the same form as (18)–(21). Because of the matrix inversions in (31)–(34), however, the number of expansion terms in subregions IIa and IIb must be equal, e.g. $M = N$. Especially for small slots and/or thick fins, this tends to cause numerical instabilities as a result of extremely high numbers to be handled by the computer. It is advisable, therefore, to run this version of the transverse resonance method on extended precision compilers as opposed to a double precision accuracy which is usually sufficient for Method 1.

The number M of expansion terms of the two field matching methods and the numbers of TE and TM modes required for the mode-matching technique in axial direction are determined by convergence analyses of the evanescent-mode resonator in Figure 1. Sufficient results are obtained with $M = 9$ and the lowest $N_h = 12$ (TE) and $N_e = 7$ (TM) modes in rectangular as well as finned waveguide sections. The numerical algorithm requires the two-dimensional problem (Section 2.2 or 2.3) to be solved first. Using the above numbers, this takes three minutes on a 20 MHz 386-comparable computer for Method 2 and five minutes for Method 1 owing to a more complicated search algorithm as discussed in the next section. Subsequently, the mode-matching technique in propagation direction (Section 2.1) requires 20 seconds per frequency point for the finned waveguide resonator shown in Figure 1. Since this algorithm is identical for both methods, no difference in CPU time is observed.

3. RESULTS

The typical behaviour of the system determinants of the two methods investigated is demonstrated in Figure 3 at the example of a W-band finned waveguide cross-section. Figure 3(a) shows the function obtained with Method 2 using only four expansion terms because of the small slot width of 50 μm. This algorithm combines the advantages of maintaining the size of the characteristic matrix regardless of the number of subregions in the x-direction[22,23] with the absence of poles. Hence, a simple sign-detecting algorithm can be used to find the zeros which, in this example, correspond to the first seven TE mode cutoff frequencies.

Figure 3(b) shows the system determinant of Method 1 using $N = 2$ and $M = 9$ expansion terms for the same structure. The calculated cutoff frequencies (zeros) are within the plotting accuracy of those in Figure 3(a). The function itself, however, looks completely different, owing to the appearance of poles. This calls for a more sophisticated and time-consuming search algorithm to detect a complete set of zeros. The problems related to the presence of the poles and possibilities of finding zeros by locating the poles have been studied in, for example, Reference 27. However, it is remarkable that the determinant function of Method 1 (matrix size $N \times N$ or even $M \times M$ if N equals M) used here as well as that of a $(M + N) \times (M + N)$ matrix in Reference 3 shows poles whereas the formulation of Method 2 using an $M \times M$ size matrix does not. Besides other, more complicated matrix formulations based on modal analysis for the evaluation of the finned waveguide mode spectrum,[28,29] Method 2 is the only one known to the author that is free of poles in its determinant function.

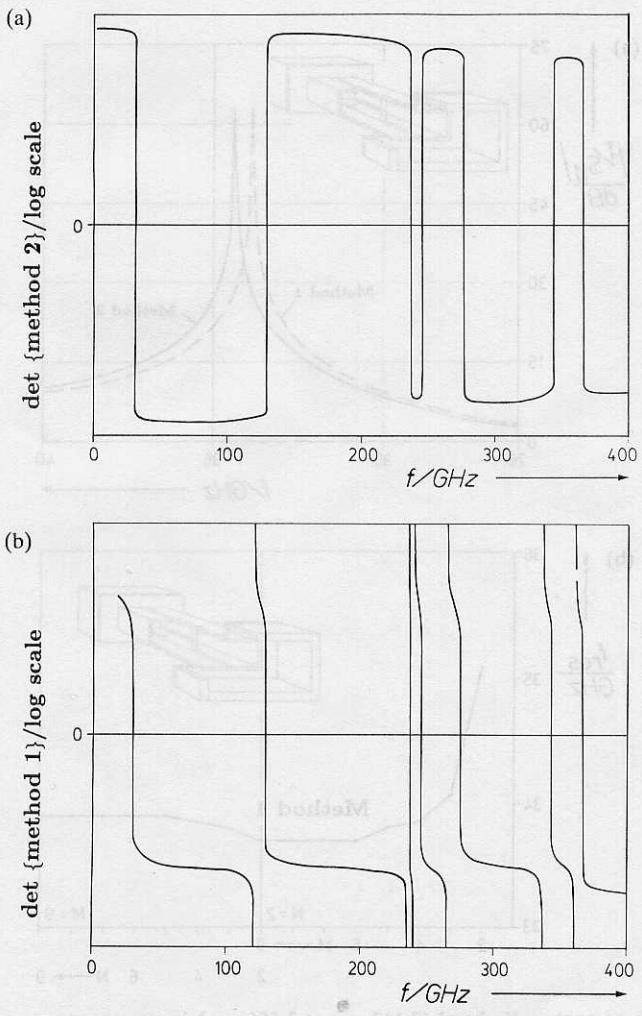

Figure 3. Typical behaviour of system determinant versus frequency demonstrated at the example of a ridged waveguide in a W-band housing ($a = 2b = 2{\cdot}54$ mm, $t = s = 50$ μm). Zeros correspond to TE-mode cutoff frequencies. (a) Method 2 (four expansion terms); (b) Method 1 (2[IIa] and 9[IIb] expansion terms)

The input return loss of a single resonator evanescent-mode filter is shown in Figure 4(a). Although the same numbers of modes are used ($N = M = 9$, $N_h = 12$, $N_e = 7$), the results obtained with the two methods for this Ka-band example differ by approximately 500 MHz (1·5 per cent) in resonant frequency. Figure 4(b) shows a convergence analysis of the resonant frequency of the complete finned waveguide resonator in Figure 4(a) with respect to the number M of modes and different modes ratios N/M used in Method 1. It is observed that different convergence levels occur, for example, for $M > 5$ if $N = 2$ and for $N > 4$ if $M = 9$. This phenomenon is known as relative convergence and has been addressed by several authors.[26,30] It should be mentioned, however, that a further increase of M and/or N does not reduce the 1·5 per cent difference between the two methods but leads from the calculations of Figure 4(b) to seriously degraded results which confirms a similar conclusion presented in Reference 30. For the many different finned waveguide structures calculated throughout this investigation, resonances computed by Method 1 were always found to be slightly lower in frequency than those obtained by Method 2 (see Figure 4(a) in Reference 20). With increasing slot width, however, they both converge to the resonant frequency of the empty evanescent-mode waveguide (see Figure 5(a), upper right).

Figure 5 demonstrates the advantage of Method 1 when structures with extremely small slots (Figure 5(a)) or thick ridges (Figure 5(b)) are computed. Owing to the fact that this procedure (dashed lines) offers the possibility of choosing the expansion term ratio according to the specified dimensions s and b (see Figure 2), the method can handle any practical ridge dimensions in waveguide. Method 2 (solid lines), however, fails for small slot widths ($s < 0{\cdot}3$ mm, Figure 5(a)) and thick ridges ($t > 1{\cdot}2$ mm, Figure 5(b)), owing to numerical errors caused by the required high

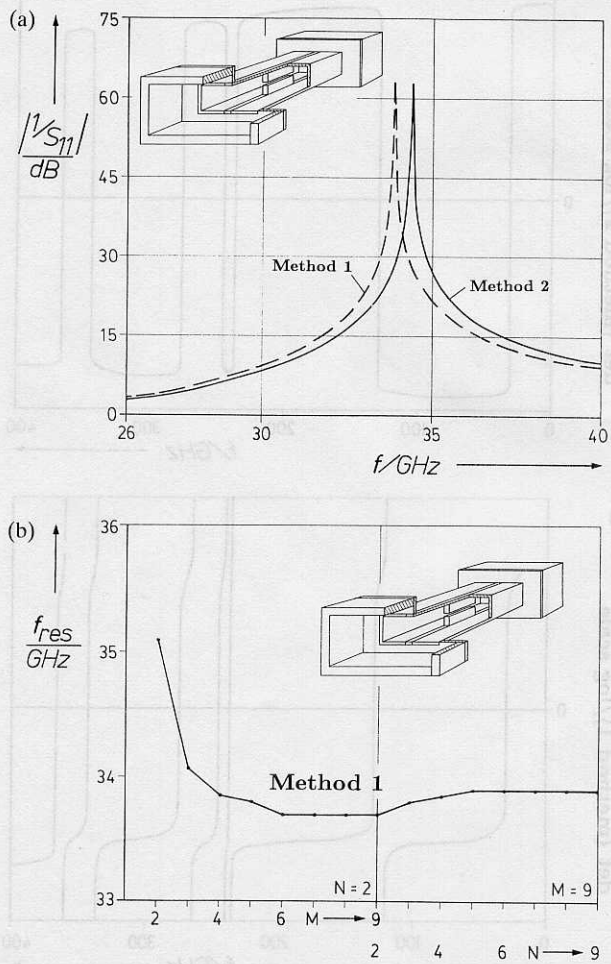

Figure 4. Finned waveguide resonator. Ka-band (7·112 mm × 3·556 mm) input–output waveguide, U-band (4·7752 mm × 2·3876 mm) evanescent-mode waveguide, $t = 0{\cdot}2$ mm, $s = 1{\cdot}2$ mm, $l_1 = l_2 = l_3 = 0{\cdot}5$ mm. (a) Input return loss: Method 1 (dashed lines); Method 2 (solid lines). (b) Convergence analysis for Method 1: resonant frequency as a function of expansion terms in subregions IIa, IIb (see equations (18)–(21)). Number of modes in axial direction kept constant at $N_h = 12$, $N_e = 7$ (see equations (3), (4))

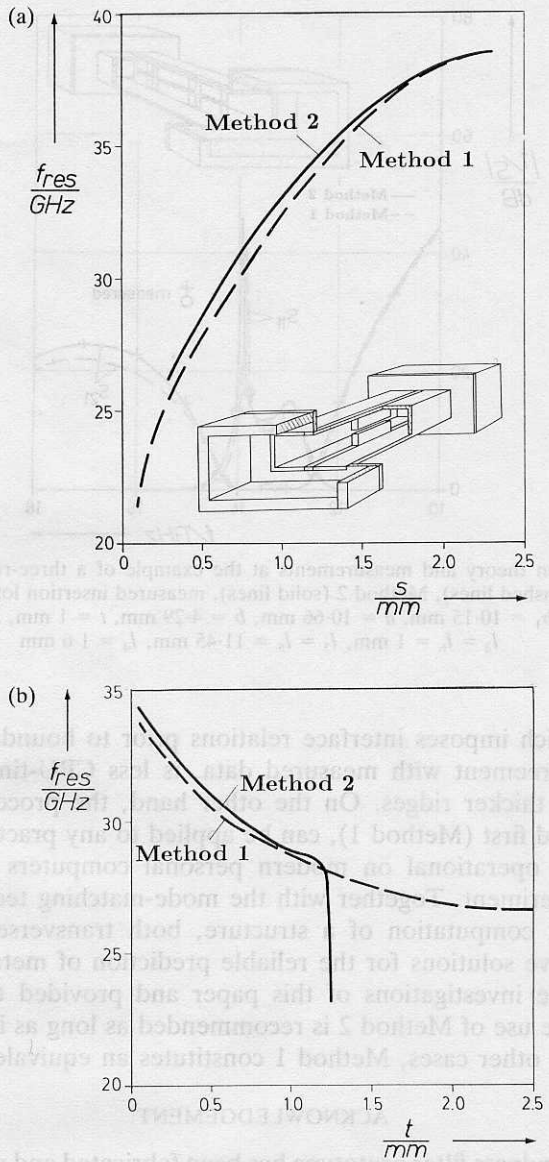

Figure 5. Resonant frequency of finned waveguide resonator versus (a) slot width s (t = 0·2 mm), (b) fin thickness t (s = 1·0 mm). Other dimensions as in Figure 4

number of expansion terms ($N = M$) in subregion IIa. For given dimensions, it is therefore advisable to verify whether or not convergence can be obtained with Method 2 without the presence of numerical instabilities.

Figure 6 compares the results of both techniques with measured data of a three-resonator bandpass filter prototype. Both approaches provide good agreement with the experiment. However, Method 2 (solid lines) performs somewhat better than Method 1 (dashed lines), especially towards higher frequencies. Again, the return loss peak calculated with Method 1 is slightly lower in frequency than that obtained by Method 2. These computations have been carried out using 20 TE, 13 TM modes, $M = 9$ expansion terms (Method 2) and $N/M = 2/9$ (Method 1). However, the software using Method 1 was still operational on 386-comparable personal computers because there were only two expansion terms in subregion IIa, while Method 2 required extended-precision mainframe support in order to cope with $M = 9$ expansion terms in that area.

4. CONCLUSIONS

The influence of different formulations of the transverse resonance field-matching technique on the three-dimensional computation of metal-finned evanescent-mode waveguide filters is investi-

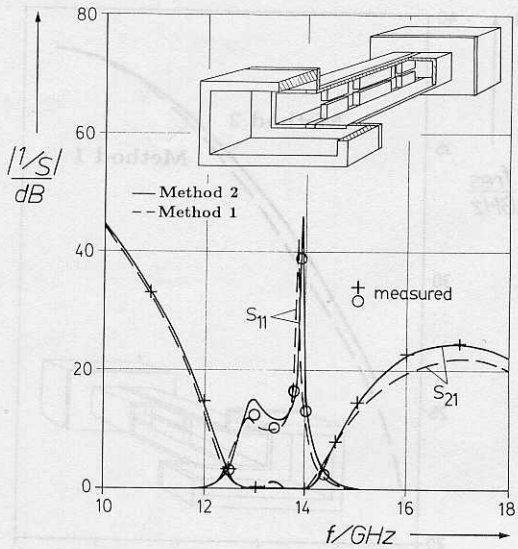

Figure 6. Comparison between theory and measurements at the example of a three-resonator evanescent-mode finned waveguide filter. Method 1 (dashed lines), Method 2 (solid lines), measured insertion loss (+), measured return loss (○). Dimensions: $a_1 = 22{\cdot}85$ mm, $b_1 = 10{\cdot}15$ mm, $a = 10{\cdot}66$ mm, $b = 4{\cdot}29$ mm, $t = 1$ mm, $s = 0{\cdot}98$ mm, $l_1 = l_7 = 0{\cdot}25$ mm, $l_2 = l_6 = 1$ mm, $l_3 = l_5 = 11{\cdot}45$ mm, $l_4 = 1{\cdot}6$ mm

gated. The method, which imposes interface relations prior to boundary conditions (Method 2) shows slightly closer agreement with measured data, is less CPU-time-consuming but fails for small slot width and/or thicker ridges. On the other hand, the procedure where the boundary conditions are considered first (Method 1), can be applied to any practical ridged or metal-finned waveguide structure, is operational on modern personal computers and is still in reasonable agreement with the experiment. Together with the mode-matching technique which leads to the modal scattering matrix computation of a structure, both transverse resonance field-matching techniques offer attractive solutions for the reliable prediction of metal-finned waveguide circuit responses. Based on the investigations of this paper and provided that an extended-precision compiler is available, the use of Method 2 is recommended as long as it is applicable to the cross-sections involved. In all other cases, Method 1 constitutes an equivalently powerful alternative.

ACKNOWLEDGEMENT

The evanescent-mode bandpass filter prototype has been fabricated and measured at the Microwave Department of the University of Bremen, Germany. The author gratefully acknowledges the support of the head of the Department, Professor Fritz Arndt, and one member of his staff, Mr. Wolfgang Robran.

REFERENCES

1. S. B. Cohn, 'Properties of ridge wave guide', *Proc. IRE*, **35**, 783–788 (1947).
2. S. Hopfer, 'The design of ridged waveguide', *IRE Trans. Microwave Theory and Techniques*, **MTT-3**, 20–29 (1955).
3. J. P. Montgomery, 'On the complete eigenvalue solution of ridged waveguide', *IEEE Trans. Microwave Theory and Techniques*, **MTT-19**, 547–555 (1971).
4. W. J. R. Hoefer and M. N. Burtin, 'Closed-form expressions for the parameters of finned and ridged waveguides', *IEEE Trans. Microwave Theory and Techniques*, **MTT-30**, 2190–2194 (1982).
5. Y. Utsumi, 'Variational analysis of ridged waveguide modes', *IEEE Trans. Microwave Theory and Techniques*, **MTT-33**, 111–120 (1985).
6. E. S. Hensperger, 'Broad-band stepped transformers from rectangular to double-ridged waveguide', *IRE Trans. Microwave Theory and Techniques*, **MTT-6**, 311–314 (1955).
7. L. Freiberg, 'An empirical design method for multisection ridge-guide transducers of large-impedance transformation', *IRE Trans. Microwave Theory and Techniques*, **MTT-9**, 263–266 (1961).
8. W. J. Getsinger, 'Ridge waveguide field description and application to directional couplers', *IRE Trans. Microwave Theory and Techniques*, **MTT-10**, 41–50 (1962).
9. H. F. Chappell, 'Waveguide low pass filter using evanescent mode inductors', *Microwave Journal*, **21**, 71–72 (1978).
10. G. Craven, 'Tuning techniques for multisection waveguide bandpass filters using evanescent modes', *Elect. Letters*, **2**, 419–420 (1966).
11. G. Graven and C. K. Mok, 'The design of evanescent mode waveguide band-pass filters for a prescribed insertion loss characteristic', *IEEE Trans. Microwave Theory and Techniques*, **MTT-19**, 295–308 (1971).

12. R. V. Snyder, 'Broadband waveguide or coaxial filters with wide stopbands, using a stepped-wall evanescent mode approach', *Microwave Journal*, **26**, 53–58 (1983).
13. A. M. K. Saad, 'Novel lowpass harmonic filters for satellite application', in *1984 IEEE MTT-S Int. Symp. Digest*, 1984, pp. 292–294.
14. Y. Konishi and H. Matsumura, 'Short end effect of ridge guide with planar circuit mounted in a waveguide', *IEEE Trans. Microwave Theory and Techniques*, **MTT-27**, 168–170 (1979).
15. N. C. Albertsen and P. Skov-Madsen, 'A compact septum polarizer', *IEEE Trans. Microwave Theory and Techniques*, **MTT-31**, 654–660 (1983).
16. J. Bornemann and F. Arndt, 'Modal-S-matrix design of optimum stepped ridged and finned waveguide transformers', *IEEE Trans. Microwave Theory and Techniques*, **MTT-35**, 561–567 (1987).
17. Q. Zhang and T. Itoh, 'Computer-aided design of evanescent-mode waveguide filter with non-touching E-plane fins', *IEEE Trans. Microwave Theory and Techniques*, **MTT-36**, 404–412 (1988).
18. R. R. Mansour, R. S. K. Tong and R. H. MacPhie, 'Simplified description of the field distribution in finlines and ridge waveguides and its application to the analysis of E-plane discontinuities', *IEEE Trans. Microwave Theory and Techniques*, **MTT-36**, 1825–1832 (1988).
19. J. Bornemann and F. Arndt, 'Optimum field theory design of E-plane finned waveguide transformers of different inner cross-sections', in *1990 IEEE MTT-S Int. Symp. Digest*, 1990, 1071–1074.
20. J. Bornemann and F. Arndt, 'Transverse resonance, standing wave and resonator formulation of the ridge waveguide eigenvalue problem and its application to the design of E-plane finned waveguide filters', *IEEE Trans. Microwave Theory and Techniques*, **38**, 1104–1113 (1990).
21. A. Wexler, 'Solution of waveguide discontinuities by modal analysis', *IEEE Trans. Microwave Theory and Techniques*, **MTT-15**, 508–517 (1967).
22. J. Bornemann, 'Rigorous field theory analysis of quasiplanar waveguides', *Proc. Inst. Elec. Eng.*, **132**, pt. H, 1–6 (1985).
23. R. Vahldieck and J. Bornemann, 'A modified mode-matching technique and its application to a class of quasi-planar transmission-lines', *IEEE Trans. Microwave Theory and Techniques*, **MTT-33**, 916–926 (1985).
24. J. Bornemann and F. Arndt, 'Calculating the characteristic impedance of finlines by transverse resonance method', *IEEE Trans. Microwave Theory and Techniques*, **MTT-34**, 85–92 (1986).
25. R. Sorrentino and T. Itoh, 'Transverse resonance analysis of fin-line discontinuities', *IEEE Trans. Microwave Theory and Techniques*, **MTT-32**, 1633–1638 (1984).
26. T. Itoh, *Numerical Techniques for Microwave and Millimeter-Wave Passive Structures*, John Wiley, New York, 1989, Ch. 9.
27. C. A. Olley and T. E. Rozzi, 'Systematic characterization of the spectrum of unilateral finline', *IEEE Trans. Microwave Theory and Techniques*, **MTT-34**, 1147–1156 (1986).
28. E. Kühn, 'A mode-matching method for solving field problems in waveguide and resonator circuits', *Arch. Elek. Übertragung*, **27**, 511–518 (1973).
29. R. R. Mansour and R. H. MacPhie, 'A unified hybrid-mode analysis for planar transmission lines with multilayer isotropic/anisotropic substrates', *IEEE Trans. Microwave Theory and Techniques*, **MTT-35**, (1987).
30. S. W. Lee, W. R. Jones and J. J. Campbell, 'Convergence of numerical solutions of iris-type discontinuity problems', *IEEE Trans. Microwave Theory and Techniques*, **MTT-19**, 528–536 (1971).

Author's biography:

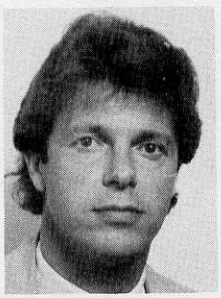

Jens Bornemann was born in Hamburg, Germany, in 1952. He received the Dipl.-Ing. and the Dr.-Ing. degrees, both in electrical engineering, from the University of Bremen, Germany, in 1980 and 1984, respectively.

For 1980 to 1983, he was a Research and Teaching Assistant in the Microwave Department at the University of Bremen, working on quasi-planar waveguide configurations and computer-aided *E*-plane filter design. After a two-year period as a consulting engineer, he joined the University of Bremen again, in 1985, where he was employed at the level of Assistant Professor. Since April 1988, he has been an Associate Professor at the University of Victoria, Victoria, BC, Canada. His curent research activities include microwave system design, active components, and problems of electromagnetic field theory.

Dr. Bornemann was one of the recipients of the A.F. Bulgin Premium of the Institution of Electronic and Radio Engineers in 1983. He is a Senior Member of IEEE, serves on the editorial board of the *IEEE Transactions on Microwave Theory and Techniques*, and has authored and co-authored more than forty technical papers.